Materials and Design 57 (2014) 269–278

Contents lists available at ScienceDirect

Materials and Design

journal homepage: www.elsevier.com/locate/matdes

Influence of probe offset distance on interfacial microstructure and mechanical properties of friction stir butt welded joint of Ti6Al4V and A6061 dissimilar alloys

Zhihua Song [a,b,c,d,*], Kazuhiro Nakata [a], Aiping Wu [b,c], Jinsun Liao [e], Li Zhou [a,1]

[a] Joining and Welding Research Institute, Osaka University, Osaka, Ibaraki 567-0047, Japan
[b] Department of Mechanical Engineering, Tsinghua University, Beijing 100084, PR China
[c] Key Laboratory for Advanced Materials Processing Technology, Ministry of Education, PR China
[d] Beijing Institute of Control Engineering, Beijing 100190, PR China
[e] Kurimoto Ltd., Osaka 559-0021, Japan

ARTICLE INFO

Article history:
Received 31 January 2013
Accepted 16 December 2013
Available online 21 December 2013

Keywords:
Friction stir butt welding
Ti/Al dissimilar joining
Probe offset distance
Interfacial microstructure
Mechanical properties

ABSTRACT

Friction stir butt welding of titanium alloy Ti6Al4V and aluminum alloy A6061-T6 with 2 mm thickness was conducted by offsetting probe edge into the titanium alloy at rotation speed of 750 rpm and 1000 rpm and welding speed of 120 mm/min. The effect of probe offset distance on the interfacial microstructure and mechanical properties of the butt joint was investigated. When the probe offset distance is not sufficient, the two alloys cannot be completely joined together, i.e. there exists no bonding or kissing bonding at the root part of joint interface. However, when the probe offset distance is too large, a great amount of intermetallic compounds are formed at the joint interface and its adjacency, leading to fracturing roughly along the joint interface during a tensile test. In a proper range of probe offset distance, sound dissimilar butt joints are produced, which have comparatively high tensile strength and fracture in heat affected zone of the aluminum alloy during a tensile test.

1. Introduction

Dissimilar joining of titanium and aluminum alloys has potential application in aerospace and automobile industry, which can reduce weight and cost (due to aluminum alloy) and improve strength, corrosion resistance and high temperature property (due to titanium alloy). However, successful welding of titanium and aluminum alloys is of challenge, because there are many differences between the two alloys in physical, chemical and metallurgical properties. The key problem is the formation of brittle intermetallic compounds (IMCs) in Ti/Al joints [1].

In recent years, laser welding [2–5], diffusion welding [6–10], friction welding [11–13] and friction stir welding (FSW) [14–20] have been attempting to join the Ti/Al dissimilar alloys. Laser welding is a promising process for joining of dissimilar metals due to its high energy density, narrow fusion zone, rapid cooling speed and consequently the limited formation of IMCs; however it is still difficult to control the formation of Ti–Al compounds at the joint interface. It may deteriorate the mechanical properties of laser beam joints of Ti/Al dissimilar alloys [2,3]. Yao et al. [6,7] reported on vacuum diffusion welding between titanium alloys and aluminum alloys. $TiAl_3$ intermetallic compounds was formed in the diffusion bonding of pure Ti/pure Al, while $Al_{18}Ti_2Mg_3$ was the unique product from the diffusion bonding of TA2/5A06. Friction welding could join dissimilar rods of titanium alloys and aluminum alloys and obtain high joint efficiency. When $Ti_2Mg_3Al_{18}$ intermetallic compound was formed in the joint interface, the joints fractured at the welded interface [11].

FSW, a novel solid-state joining technology developed by the welding institute (TWI) in 1991, is also a potential choice for dissimilar joining of different alloys. Chen and Nakata [14] reported on friction stir lap welding between pure titanium and aluminum alloy, and new phase of $TiAl_3$ formed at the joint interface by Al–Ti diffusion reaction. Dressler et al. [16] reported that titanium alloy Ti6Al4V and aluminum alloy AA2024-T3 could be successfully joined by friction stir butt welding. A small band next to the joint interface was recrystallized on the titanium side of the joint. Since IMCs were not observed at the most part of the interface, the principal bonding mechanism of the interface was assumed to be diffusion of atoms. Bang et al. [17] researched FSW of Ti6Al4V and AA6061-T6 dissimilar alloys with 5 mm thickness using a unique shaped tool with a circular truncated cone of the probe, but the

* Corresponding author at: Joining and Welding Research Institute, Osaka University, Osaka, Ibaraki 567-0047, Japan. Tel.: +81 06 68798668; fax: +81 06 68798658.
E-mail address: songzh07@gmail.com (Z. Song).
[1] This author is now working with School of Materials Science and Engineering, Harbin Institute of Technology at Weihai.

0261-3069/$ - see front matter © 2014 Elsevier Ltd. All rights reserved.
http://dx.doi.org/10.1016/j.matdes.2013.12.040

ultimate tensile strength of the joint was 134 MPa, approximately 35% of the aluminum alloy base metal tensile strength. The reason for the low strength of weld joint was supposed to be insufficient stirring. In the probe root area with sufficient stirring, the stir zone (SZ) was composed of fine recrystallized grains of aluminum alloy and titanium alloy fragments; the joint interface revealed very complicate sequence including lamellar structure with Al and Ti–V. IMCs were neither observed at the joint interface, similar to the result reported by Dressler et al. [16]. Aonuma and Nakata [18] investigated butt joining of titanium alloy to aluminum alloy via FSW, and the joints mainly fractured in the mixed region of titanium alloy and aluminum alloy at the joint interface, where existed an IMC layer of $TiAl_3$. Chen et al. [19] researched the friction stir welded joint of Al/Ti dissimilar alloys, where zinc was added as the middle layer material. The joint became more brittle, because $TiAl_3$ and $Zn_{0.69}Ti_{0.31}$ intermetallic compounds were detected in the center region.

Although there are a few studies about friction stir butt welding of Ti/Al dissimilar alloys as mentioned above, the influence of probe offset distance on the joint formation has not been studied, and the joining mechanism is still unclear. In the present study, the titanium alloy Ti6Al4V and aluminum alloy A6061-T6, which are widely used in industries, are butt-welded via FSW; the influence of probe offset distance on interfacial microstructures and mechanical properties of the joints is researched. The joining mechanism of the interface is also being discussed.

2. Experimental details

Ti6Al4V and A6061-T6 plates with dimensions of 150 mm × 75 mm × 2 mm were used in the present study. The chemical compositions and mechanical properties of the two alloys are shown in Table 1. Friction stir butt welding of titanium alloy and aluminum alloy was conducted by offsetting probe edge into the titanium alloy, as illustrated by Fig. 1. The titanium alloy was positioned on the advancing side and the aluminum alloy was on the retreating side. The welding tool for FSW was made from a WC-Co based alloy and consisted of a concave shoulder of 15 mm diameter and a cylinder probe of 1.9 mm length and 6 mm diameter. The probe was inserted mainly on the aluminum alloy side and the probe edge was slightly offset into the titanium alloy. The probe offset distance was selected to be 0–1.2 mm in the present study. Therefore, the stirring action of the probe mainly happened in the aluminum alloy part of the joint. The detailed welding parameters are given in Table 2. Before welding, the joint surface of the titanium and aluminum alloys was machined by a milling machine and degreased with acetone.

After welding, the joints were cross-sectioned perpendicularly to the welding direction for metallographic analysis. The microstructures of joints were examined by optical microscope (OM) and scanning electron microscope (SEM, JEOL: JSM-6500F) equipped with an energy-dispersive X-ray spectrometer (EDS). The specimens for OM were etched with Keller's etchant (1.0 ml HF + 1.5 ml HCl + 2.5 ml HNO_3 + 95 ml H_2O) according to ISO/TR 16060: 2003 [21]. Backscattered electron images of SEM were used to analyze the IMCs at the joint interface. The microstructures at the joint interface were also characterized with electron backscatter diffraction (EBSD). The samples for EBSD analysis were prepared using an ion polisher (JEOL SM-09010).

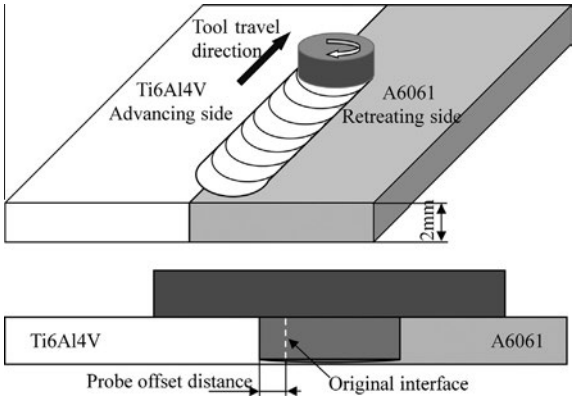

Fig. 1. Schematic illustration of friction stir butt welding of Ti6Al4V/A6061 dissimilar alloys.

Tensile specimens were cross-sectioned perpendicular to the welding direction. The strength of the joint was evaluated via tensile test at room temperature according to ISO 6892: 1998 [22]. The tensile test was carried out using a testing machine INSTRON 5500 at a crosshead speed of 0.1 mm/min. Three specimens were tested for each welding condition, and the average value was used to evaluate the tensile strength of the joint. Fracture surfaces of joints were analyzed using SEM-EDS and X-ray diffraction (XRD) after the tensile test. Hardness measurement was performed on the metallographic specimens crossing the joints at mid thickness using a Vickers indenter and a load of 490 mN, and the distance between two neighboring indentations was 500 μm.

3. Result and discussion

3.1. Macrostructure and microstructure of joint

Appearance and cross-section macrostructure of Ti6Al4V/A6061 FSW joints with various probe offset distances at 750 rpm and 1000 rpm are shown in Figs. 2 and 3, respectively. The magnified images of the region around the joint interface are given in Fig. 4. It can be seen that the appearances of the joints are similar at different probe offset distances under rotation speeds of 750 rpm and 1000 rpm. The probe offset distance has a great influence on the formation of joint. At the rotation speed of 750 rpm, the titanium and aluminum plates are well bonded together at the upper part of the joint but no bonding or kissing bonding exists at the root part of the joint interface when probe offset distance is 0.6 mm or smaller. The two plates are soundly joined together when the offset is increased to 0.9–1.2 mm. With the rotation speed increased to 1000 rpm, the two plates are soundly joined together when the probe offset distance exceeds 0.6 mm (Fig. 4). A swirl-like structure is formed in the stir zone (SZ) next to the joint interface at the upper part of the joint, and the area of swirl-like

Table 1
Chemical compositions and mechanical properties of base materials (wt.%).

Alloys	Ti	Al	Si	Fe	Cu	Mn	Mg	Cr	Zn	V	C	O	N	H	Tensile strength σ_b (MPa)	Yield strength $\sigma_{0.2}$ (MPa)	Elongation (%)
A6061-T6	0.02	Bal.	0.63	0.29	0.27	0.07	1.00	0.17	0.01	–	–	–	–	–	318	289	11.2
Ti6Al4V	Bal.	6.21	–	0.135	–	–	–	–	–	3.93	0.023	0.126	0.003	0.002	952	877	12.6

Table 2
Parameters for dissimilar butt-welding of Ti6Al4V and A6061.

Tool material		WC-Co
Tool geometry	Shoulder diameter (mm)	15
	Probe diameter (mm)	6
	Probe length (mm)	1.9
Axial tool force (kN)		7.5
Tool rotation speed (rpm)		750, 1000
Welding speed (mm/min)		120
Tilt angle (degree)		3
Probe edge offset into the Ti alloy (mm)		0, 0.3, 0.6, 0.9, 1.2

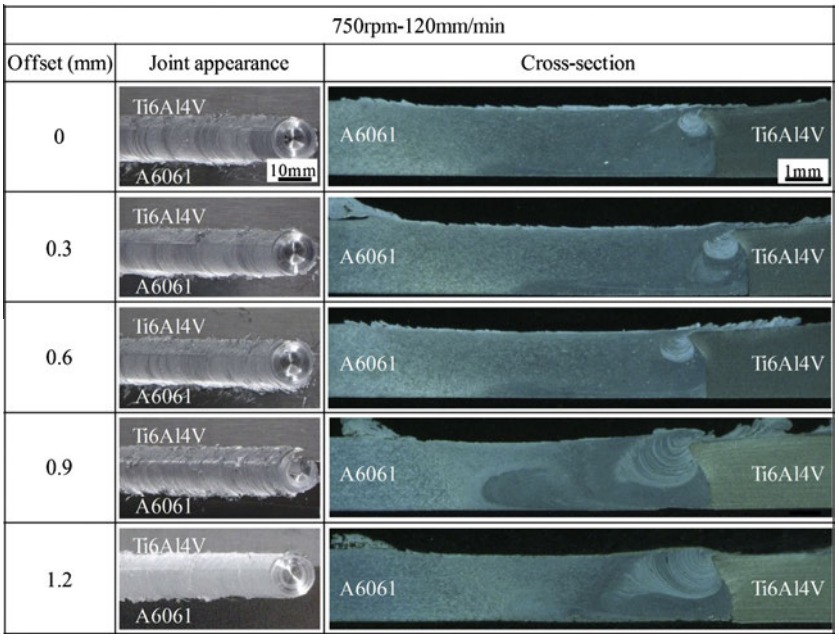

Fig. 2. Surface appearance and cross-section macrostructure of joints with various probe offset distances at 750 rpm.

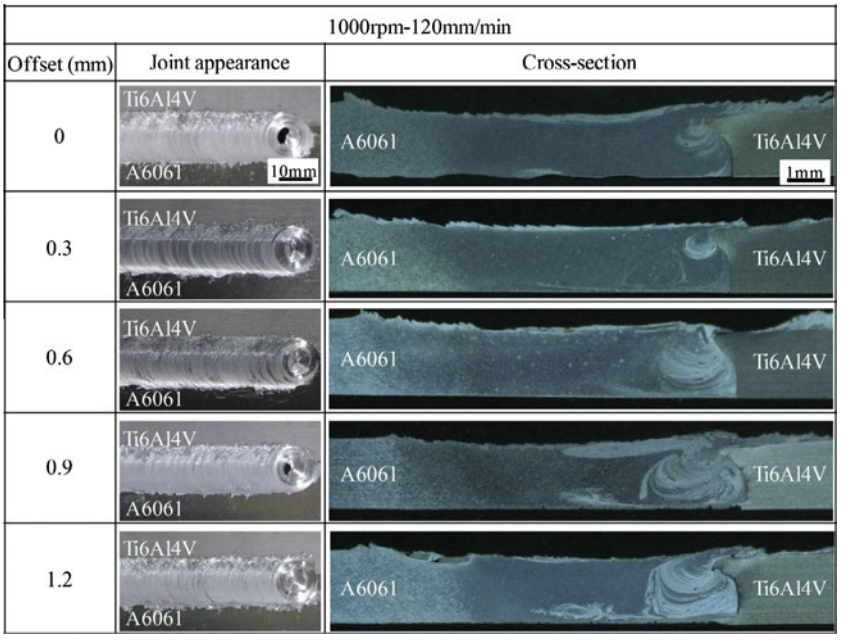

Fig. 3. Surface appearance and cross-section macrostructure of joints with various probe offset distances at 1000 rpm.

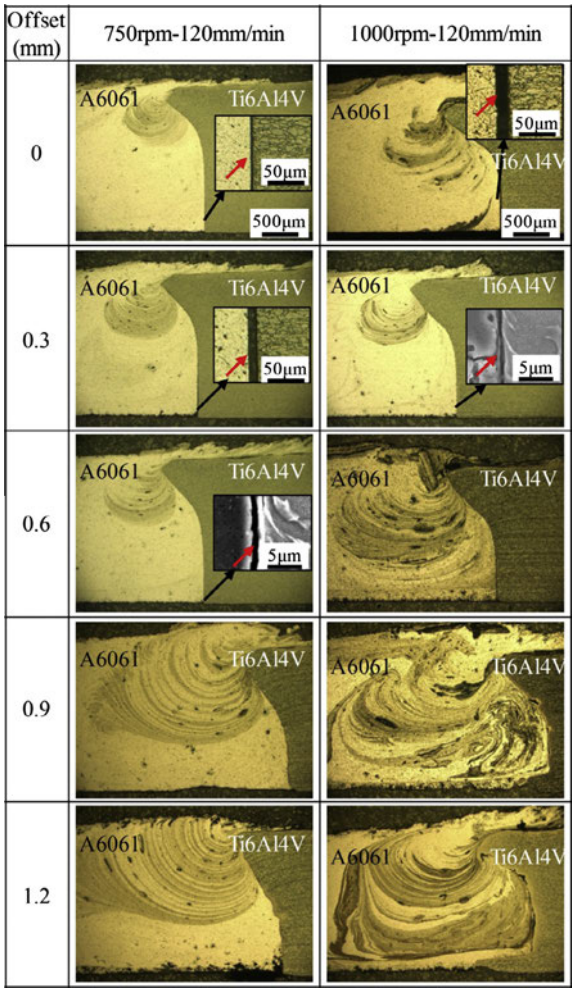

Fig. 4. Magnified images of the region around the joint interface with various probe offset distances.

structure becomes larger with increasing rotation speed and/or probe offset distance (Figs. 2 and 3). Fig. 5 shows the element mapping result of joints with various probe offset distances at 1000 rpm. It is clear that the swirl-like structure is produced by titanium alloy particles or fragments, which are chipped from titanium alloy plate and stirred into SZ by the probe during FSW. With the probe offset distance and/or rotation speed of the tool ncreased, the quantity of chipped titanium alloy particles is increasing, and the area of swirl-like structure is becoming larger.

Fig. 6 shows the microstructures in different areas at the cross-section of the joint under the tool rotation speed of 1000 rpm and probe offset distance of 0.9 mm. The SZ occurs mainly on the aluminum alloy part of joint, because the probe was inserted mainly on the aluminum alloy side. The middle region of SZ is composed of recrystallized aluminum alloy grains (Fig. 6e), and the grain size in this region becomes significantly smaller compared with the initial grain size of aluminum alloy base metal (BM) (Fig. 6b). The right region of SZ close to the joint interface, is mainly composed of recrystallized aluminum alloy grains and titanium alloy fragments, which form lamellar-structure (Fig. 6f). The microstructures in this region will be further described later. From Fig. 6g–i, which exhibit the microstructures at the upper, middle and root parts of the joint interface, respectively, it can be found that titanium alloy fragments are present in the SZ next to the joint interface through the thickness direction. This indicates that the probe stirred the titanium alloy across the whole thickness. The titanium alloy adjacent to the joint interface (Fig. 6i) seems to be different from the titanium alloy base metal (Fig. 6j). Severe plastic deformation occurs at the titanium alloy adjacent to the joint interface (Fig. 6i). When the probe offset distance increased to 1.2 mm, the microstructure at the upper, middle and root parts of the joint interface are shown in Fig. 7. The plastic deformation is severer at the titanium alloy adjacent to the joint interface than that of 0.9 mm probe offset distance. More titanium fragments or particles are stirred into the SZ next to the joint interface, especially at the root area of joint interface (Fig. 7c).

Fig. 8 shows the element mapping result of the middle region of SZ, the same region as shown in Fig. 6e. The particles in the middle region of SZ are mainly composed of Mg and Si. These particles are considered to be β-Mg_2Si [23–25]. It can be believed from Fig. 8 that titanium alloy is not stirred into the middle region of the SZ. Therefore, the SZ (from the middle region to aluminum alloy side), the thermo-mechanically affected zone (TMAZ) and the heat affected zone (HAZ) on the retreating side (i.e. the left side of Fig. 6) are similar to those observed on conventional FSW joint of A6061 alloy [26–28]. That is to say, these regions are not markedly affected by the titanium alloy.

3.2. Interfacial microstructure

The detailed microstructures next to the joint interface under the tool rotation speed of 1000 rpm and probe offset distance of

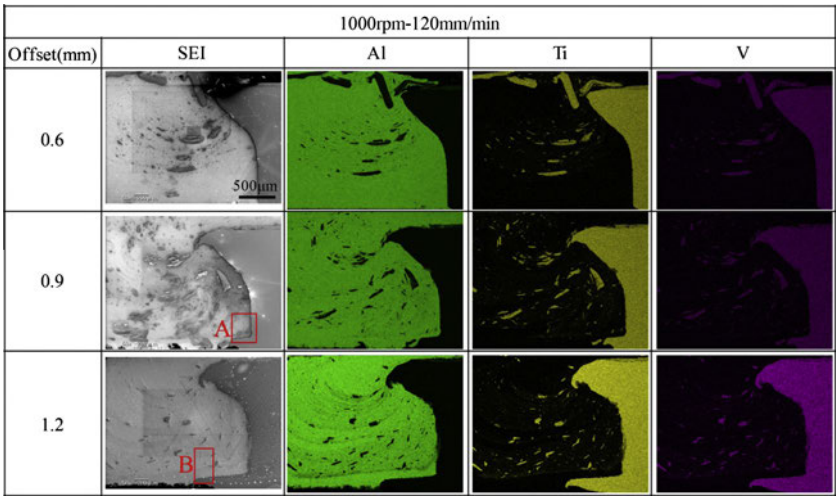

Fig. 5. Element mapping result of joints with various probe offset distances at 1000 rpm.

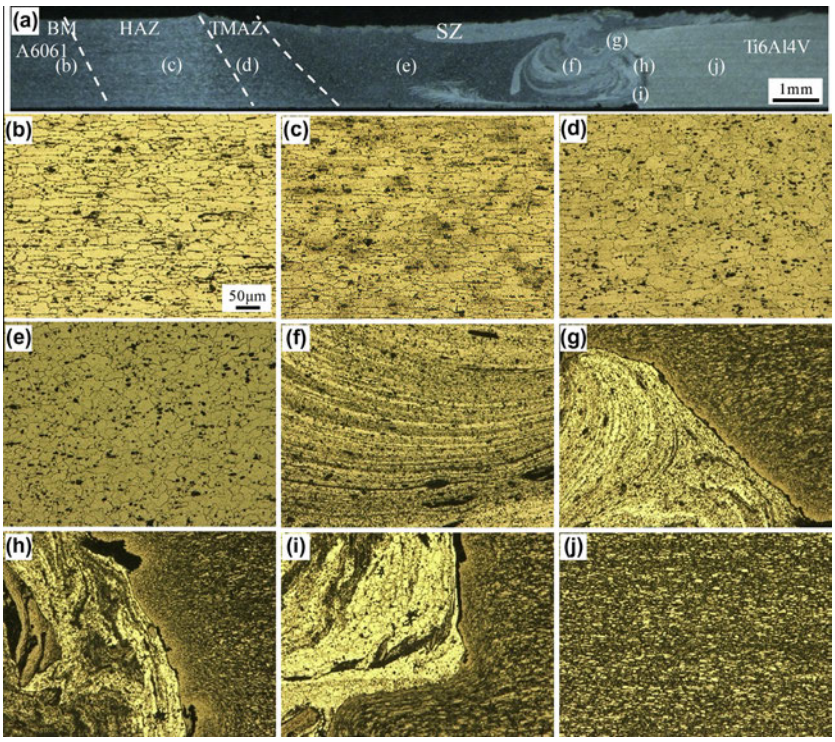

Fig. 6. Microstructure of the joint (1000 rpm–0.9 mm probe offset distance): (a) cross-section, (b) BM of A6061, (c) HAZ of A6061, (d) TMAZ of A6061, (e) middle region of SZ, (f) SZ close to the joint interface, (g) upper area of the interface, (h) middle area of the interface, (i) root area of the interface and (j) BM of Ti6Al4V.

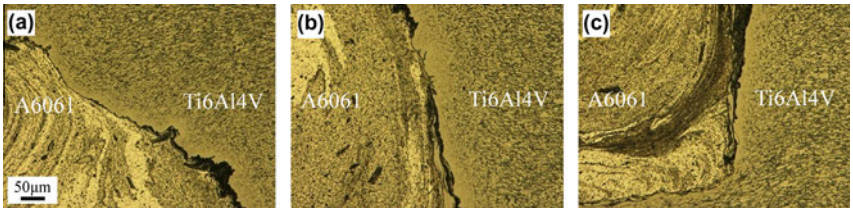

Fig. 7. Microstructure of the joint (1000 rpm–1.2 mm probe offset distance): (a) upper area of the interface, (b) middle area of the interface and (c) root area of the interface.

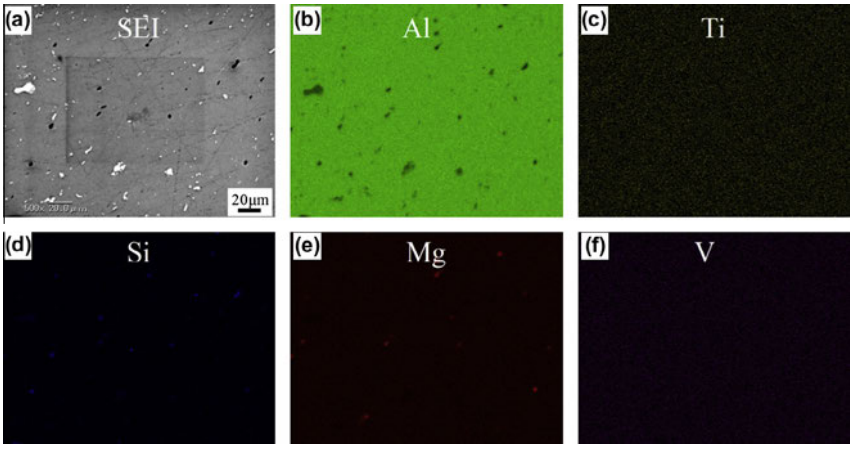

Fig. 8. Element mapping result of the middle region of SZ in Fig. 6e: (a) SEI, (b) Al, (c) Ti, (d) Si, (e) Mg and (f) V.

0.9 mm are displayed in Fig. 9. It can be clearly observed that compared with the titanium alloy base metal (Fig. 9d), the titanium alloy close to the interface are severely deformed at the upper, middle and root parts in the thickness direction due to the stirring action of the probe and/or pressing effect of the shoulder (Fig. 9a–c). In the region adjacent to the interface, a narrow band is observed, where the equiaxed primary α and β grains have been elongated. The width of this band is about 6–10 μm. Recrystallization is suggested to occur and extremely fine grains are produced in the band [16], since it experiences severe plastic deformation

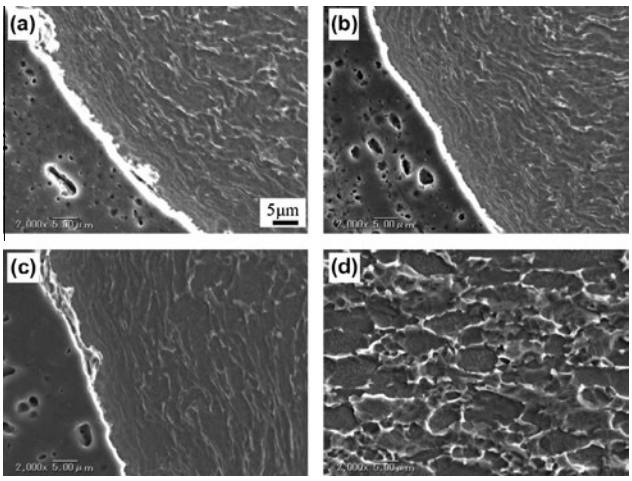

Fig. 9. Magnified SEM image next to the joint interface (1000 rpm–0.9 mm probe offset distance): (a) upper area of the interface, (b) middle area of the interface, (c) root area of the interface and (d) BM of Ti6Al4V.

and relatively high temperature during FSW; however, the fine grains cannot be clearly distinguished with SEM in the present work.

Since welding defects are prone to happening at the root part of the joint interface, it is useful to research the flow behavior and microstructures in this region. Fig. 10 gives EBSD phase maps of the region around the joint interface with 1000 rpm in rotation speed and 0.9 mm in probe offset distance. The grains on the aluminum alloy side next to the joint interface are significantly fine. There are some black areas on the aluminum alloy side, and the region on the titanium alloy side close to the joint interface is also black (Fig. 10a). When the probe offset distance is increased to 1.2 mm, the black areas on the aluminum alloy side become larger, as shown in Fig. 11. It is conceivable that the black areas on the aluminum side may be the Ti–Al compounds resulted from the reaction of Ti and Al atoms, or the titanium alloy fragments themselves with extremely fine grains may be too small to be distinguished by EBSD resulted from dynamic recrystallization due to severe plastic deformation [29]. As mentioned above (Figs. 5 and 6), titanium alloy fragments are chipped and stirred into the aluminum alloy by the stirring action of the probe during FSW. It can also be seen from Figs. 10 and 11 that the image of α titanium is clearer than β titanium on titanium alloy side slightly away from joint interface. This is probably because the grain size of β titanium is much smaller, as compared with that of α titanium.

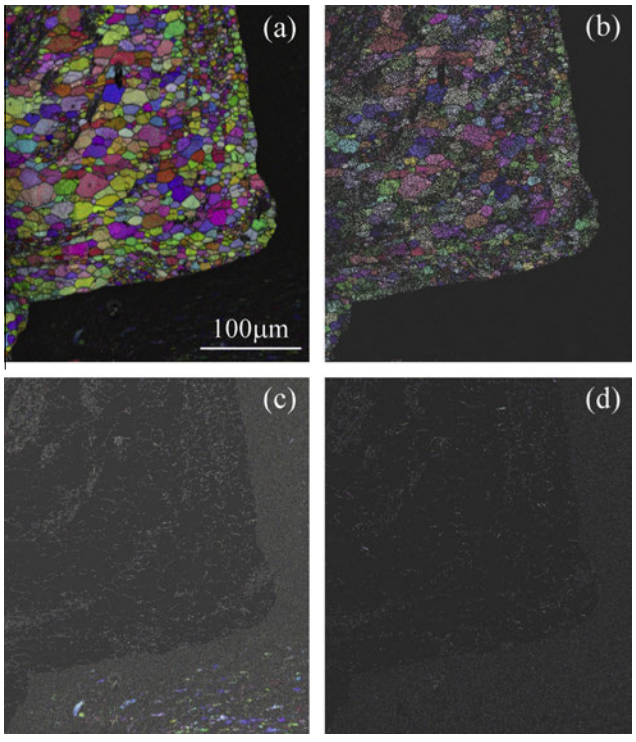

Fig. 10. EBSD analysis result of the joint interface (1000 rpm–0.9 mm probe offset distance) in zone A indicated in Fig. 5: (a) composed image, (b) image of aluminum, (c) image of α titanium and (d) image of β titanium.

In order to identify the phases in these black areas, the elemental compositions in the black areas are analyzed with EDS. Fig. 12 shows a magnified EBSD image at the joint interface and its corresponding electron image, and the elemental compositions at points 1 through 10 shown in Fig. 12 are given in Table 3. The elemental compositions at points 1, 2 and 8 with white color in Fig. 12b are close to the composition of titanium alloy base metal, indicating that the areas with white color are titanium alloy. It should be noted that point 8 shown in Fig. 12a is taken from the black area on the aluminum alloy side, and the elemental composition analysis result corroborates that this black area is a titanium alloy fragment. The elemental compositions at points 3, 4 and 7 with dark color are close to the composition of aluminum alloy base metal. The elemental compositions at points 5, 6 and 10 with light gray color in Fig. 12b are close to the composition of $TiAl_3$, which suggests the formation of $TiAl_3$. The grains in these areas are extremely small according to Fig. 12a. The proportion of titanium and aluminum atoms at point 9 is close to 1:1, which is implies that TiAl may be formed in this area.

Fig. 13 gives back-scattered electron images of interfacial microstructure of joints with various probe offset distances while the rotation speed is 1000 rpm. The observed position is in the middle-thickness of the joint. When the probe offset distance is 0.6 and 0.9 mm, it can be suggested that an IMC layer is formed at the joint interface according to the image contrast, and the thickness of IMC layer is less than 0.5 μm. However, the IMC layer is very thick and complex when the probe offset distance is increased to 1.2 mm. The titanium alloy (white color) and IMC layers (gray color) appear alternately as lamellar-structures. Besides, some microcracks are found in the IMC layers (Fig. 13c), which will be the brittle fracture initiation in the course of tensile test.

3.3. Hardness

The hardness profiles of cross-section of the joints with 0.9 and 1.2 mm in probe offset distance and 1000 rpm in rotation speed are presented in Fig. 14. The hardness is about 370 HV on the titanium alloy side. A sharp decrease to approximately 100 HV occurs at the interface of titanium and aluminum alloy, which is close to the hardness of aluminum alloy base metal. Hardness values in the SZ are not constant and the hardness is higher in the region next to the interface due to some titanium alloy fragments stirred into the aluminum alloy. Since more titanium particles are stirred into the aluminum alloy when the probe offset distance is 1.2 mm, the hardness in the SZ next to the interface is slightly higher than when it is 0.9 mm. Hardness in the SZ on the aluminum alloy side is lower than that of aluminum alloy base metal, because FSW creates a softened region around the weld center in precipitation-hardened aluminum alloys [26,27]. It was suggested hardness profile was strongly affected by precipitate distribution rather than grain size in the weld and such a softened region is caused by coarsening and dissolution of strengthening precipitates β" during the thermal cycle of the FSW [23,24,26]. The minimum hardness of

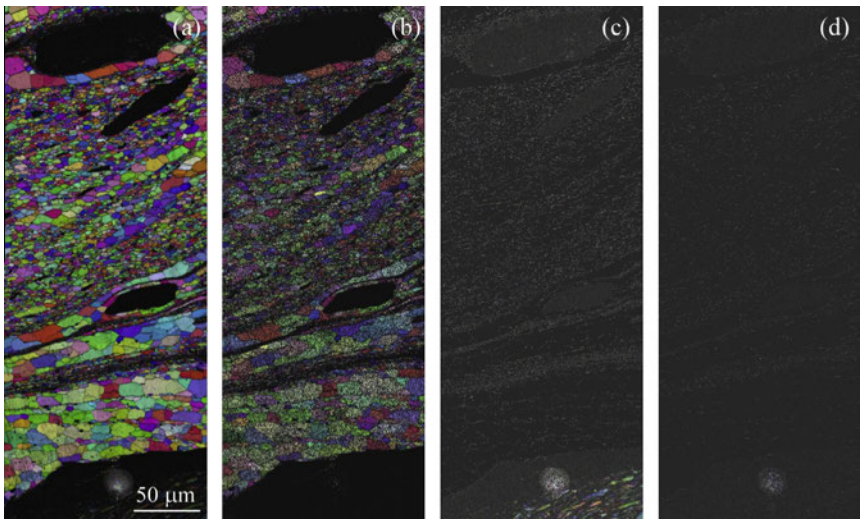

Fig. 11. EBSD analysis result of the joint interface (1000 rpm–1.2 mm probe offset distance) in zone B indicated in Fig. 5: (a) composed image, (b) image of aluminum, (c) image of α titanium and (d) image of β titanium.

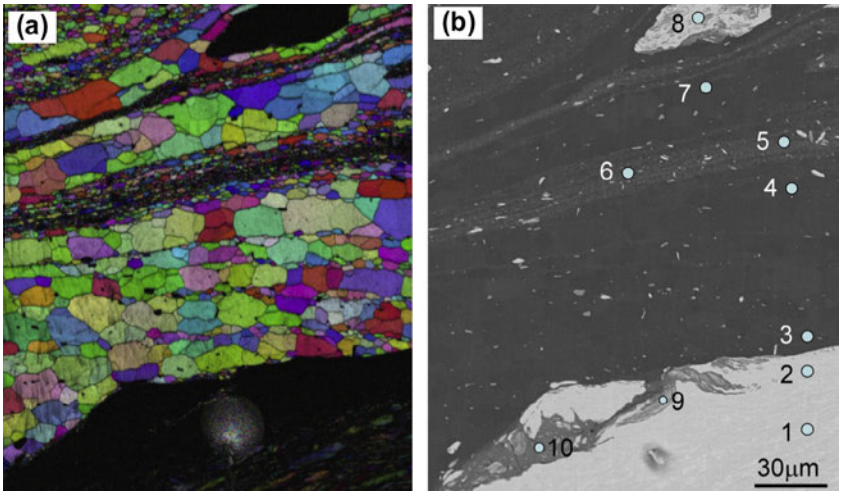

Fig. 12. Magnified EBSD image and back-scattered electron image at the joint interface (1000 rpm–1.2 mm probe offset distance): (a) EBSD image and (b) back-scattered electron image.

Table 3
Elemental compositions at points 1 through 10 shown in Fig. 12 (at.%).

Point	Al	Ti	V	Si
1	10.19	87.53	2.27	0.02
2	9.31	87.48	3.09	0.12
3	99.67	0.33	–	–
4	99.92	0.08	–	–
5	79.27	18.24	0.83	1.66
6	68.96	28.71	1.17	1.16
7	99.78	0.07	0.07	0.08
8	10.49	86.82	2.65	0.04
9	50.73	46.67	1.65	0.95
10	75.70	22.41	0.80	1.09

about 60 HV is observed in the HAZ, where β" precipitates are dissolved and coarsened Mg_2Si particles are precipitated [23].

3.4. Tensile strength and fracture analysis

The tensile strength of the joints with 750 rpm and 1000 rpm is shown in Fig. 15. It is found that the probe offset distance has a great influence on the tensile strength of joints. When rotation speed is 750 rpm, the tensile strength of the joints with probe offset distance of 0.9 mm and 1.2 mm are 192 MPa and 193 MPa, respectively. It can be seen that all tensile specimens fracture in the HAZ of aluminum alloy after tensile test (Fig. 15a and b).

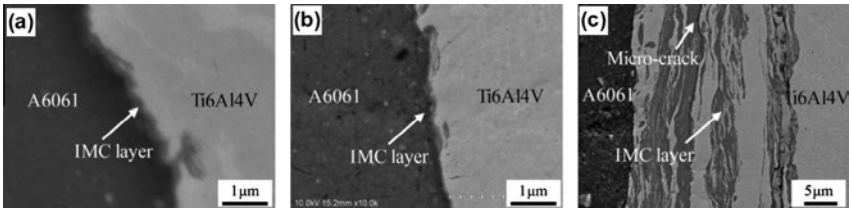

Fig. 13. Back-scattered electron images of interfacial microstructure of joints at 1000 rpm with various probe offset distances: (a) 0.6 mm, (b) 0.9 mm and (c) 1.2 mm.

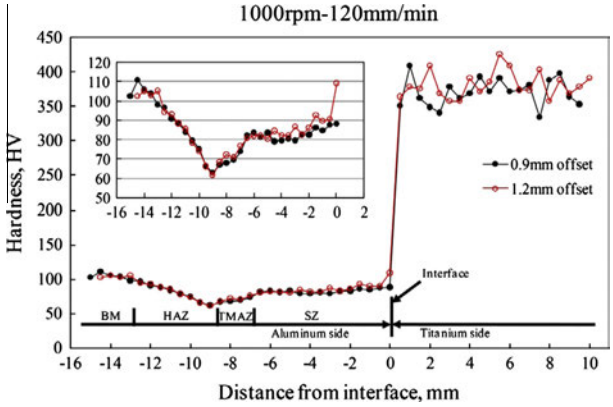

Fig. 14. Hardness profiles of cross-section of the joints with 0.9 and 1.2 mm in probe offset distance and 1000 rpm in rotation speed.

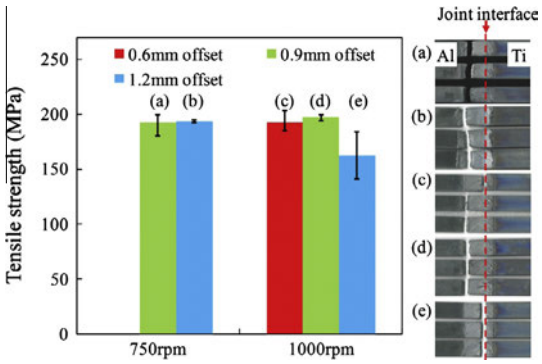

Fig. 15. Tensile strength and top surface of specimens after tensile test.

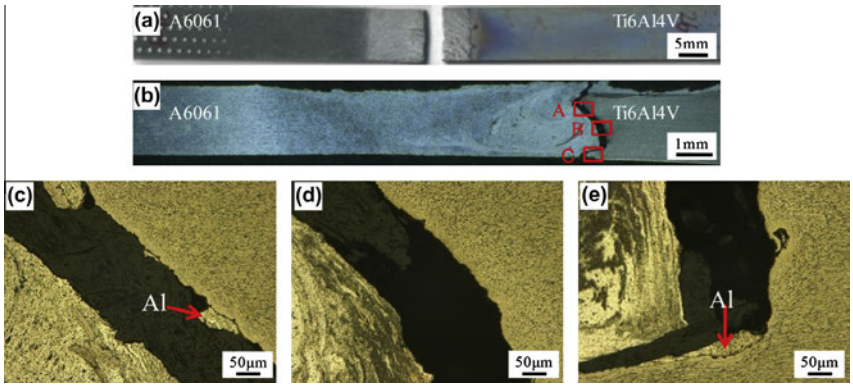

Fig. 16. Specimen after the tensile test (1000 rpm–1.2 mm probe offset distance): (a) top surface of tensile specimen, (b) optical image of a cross-section of joint, (c) zone A, (d) zone B and (e) zone C.

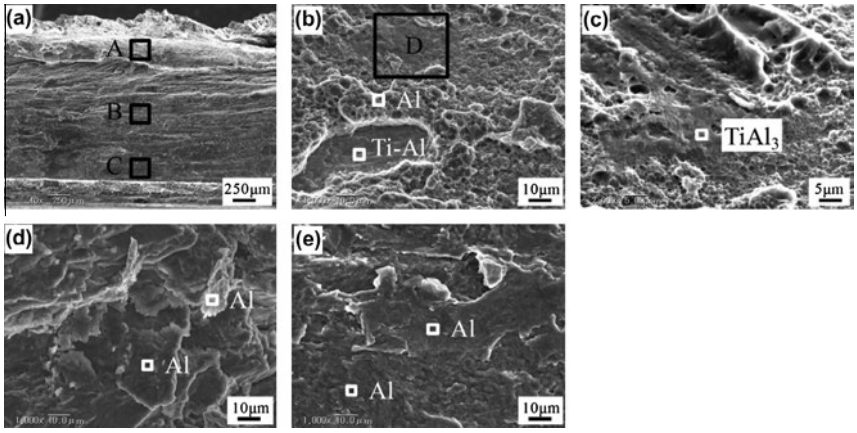

Fig. 17. Fracture surface from titanium alloy side of the joint (1000 rpm–1.2 mm probe offset distance): (a) overview of the surface, (b) zone A, (c) zone D, (d) zone B and (e) zone C.

When the rotation speed is 1000 rpm, tensile strength of the joints with probe offset distances of 0.6 mm and 0.9 mm are at the same level as that of the joints obtained at rotation speed of 750 rpm; however, as the probe offset distance is increased to 1.2 mm, tensile strength of the joint decreases obviously. As the probe offset distance is 0.9 mm, the highest average tensile strength of the joint is 197 MPa, which is 62% of aluminum alloy base metal. Three specimens fracture in the HAZ of aluminum alloy. The FSW joint exhibits a reduced strength due to the hardness loss in the HAZ compared to the aluminum alloy base metal. The fracture occurs at the location where the hardness is the lowest, i.e. the HAZ of aluminum alloy (Fig. 15). Clearly, the fracture mode of the FSW joints with the probe offset distance of 0.9 mm is controlled by the lowest hardness [28,30].

As the probe offset distance is increased to 1.2 mm while the rotation speed is 1000 rpm, however, the tensile strength has a sharp decrease to 162 MPa, and the joint fractures along the interface of the joint. The optical images of cross-section of the joint

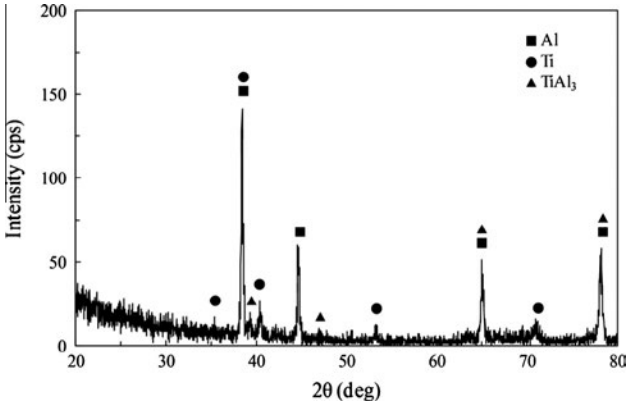

Fig. 18. XRD spectrums from the fracture surface of titanium side (1000 rpm–1.2 mm probe offset distance).

after the tensile test are shown in Fig. 16. It is clear that the joint fractures roughly along the interface between the titanium alloy and the aluminum alloy, although some aluminum alloy is observed on the titanium alloy side. The sharply decreased strength of the joint is due to the microcracks existing in the IMC layers, which leads to brittle fracture along the joint interface [18].

Fig. 17 shows fracture surface from titanium alloy side of the joint with 1000 rpm in rotation speed and 1.2 mm in probe offset distance. The magnified SEM images of zone A, B, C and D are also presented. EDS analysis shows that the compositions at the surface of these regions are close to Al, $TiAl_3$, and other Ti–Al compounds. XRD spectrums from fracture surfaces of titanium alloy also reveal that $TiAl_3$ is formed in the joint interface (Fig. 18). It was suggested that the IMC layer of $TiAl_3$ is formed during FSW of titanium alloy with aluminum alloy [14,18]. The microcrack formation is mainly because of the brittleness of the $TiAl_3$ and very thick and complex IMC layer when the probe offset distance is increased to 1.2 mm.

The main joining mechanism of Ti6Al4V/A6061 dissimilar FSW joint is suggested to be that the formation of IMCs, such as $TiAl_3$, at the interface connects titanium and aluminum plates together (Figs. 12 and 13). The joints fracture at the aluminum alloy if proper welding parameters are selected (Fig. 15), demonstrating that the bonding strength at the titanium–aluminum joint interface is higher than the strength of A6061 FSW joint. $TiAl_3$ detected from the fracture surface corroborates that $TiAl_3$ is formed at the joint interface during FSW. This result is similar to Aonuma's work [18].

4. Conclusions

Friction stir welding of titanium alloy Ti6Al4V and aluminum alloy A6061-T6 with 2 mm thickness was conducted. The probe was inserted mainly on the aluminum alloy side and the probe edge was slightly offset into the titanium alloy. The effect of probe offset distance on interfacial microstructure and mechanical property of the dissimilar butt joint was investigated. The results can be summarized as follows.

(1) FSW of Ti6Al4V/A6061 dissimilar alloys by offsetting probe edge into the titanium alloy can produce sound joints with good appearance under welding conditions of 750 rpm and 1000 rpm in rotation speed and 120 mm/min in welding speed, provided that a proper offset distance is selected.

(2) The probe offset distance has a great influence on the interfacial microstructures and mechanical properties of joints. When the probe offset distance is not sufficient, there exists no bonding or kissing bonding at the root part of joint interface. When the probe offset distance is too large, however, a great amount of IMCs are formed at the joint interface and its adjacency, leading to fracturing roughly along the joint interface during a tensile test. When the probe offset distance is proper, sound dissimilar butt joints are produced, which have comparatively high tensile strength and fracture at HAZ of the aluminum alloy during a tensile test.

(3) The Ti–Al compounds, including $TiAl_3$, are formed at the joint interface and its adjacency. The main joining mechanism of Ti6Al4V/A6061 dissimilar alloys via FSW is the formation of Ti–Al compounds at the joint interface, which connect Ti6Al4V and A6061 plates together.

References

[1] Chularis AA, Kolpachev AB, Kolpacheva OV, Tomashevskii VM. Electron structure and properties of intermetallic compounds in titanium-metal dissimilar joints. Weld Int 1995;9:812–4.
[2] Möller F, Grden M, Thomy C, Vollertsen F. Combined laser beam welding and brazing process for aluminium titanium hybrid structures. Phys Proc 2011;12(Part A):215–23.
[3] Vaidya WV, Horstmann M, Ventzke V, Petrovski B, Koçak M, Kocik R, et al. Improving interfacial properties of a laser beam welded dissimilar joint of aluminium AA6056 and titanium Ti6Al4V for aeronautical applications. J Mater Sci 2010;45:6242–54.
[4] Song Z, Nakata K, Wu A, Liao J. Interfacial microstructure and mechanical property of Ti6Al4V/A6061 dissimilar joint by direct laser brazing without filler metal and groove. Mater Sci Eng A 2013;560:111–20.
[5] Chen S, Li L, Chen Y, Dai J, Huang J. Improving interfacial reaction nonhomogeneity during laser welding–brazing aluminum to titanium. Mater Des 2011;32:4408–16.
[6] Yao W, Wu AP, Zou GS, Ren JL. Formation process of the bonding joint in Ti/Al diffusion bonding. Mater Sci Eng: A 2008;480:456–63.
[7] Yao W, Wu AP, Zou GS, Ren JL. 5A06/TA2 diffusion bonding with Nb diffusion-retarding layers. Mater Lett 2008;62:2836–9.
[8] Alhazaa AN, Khan TI. Diffusion bonding of Al7075 to Ti–6Al–4V using Cu coatings and Sn–3.6Ag–1Cu interlayers. J Alloy Compd 2010;494:351–8.
[9] Wilden J, Bergmann JP. Manufacturing of titanium/aluminium and titanium/steel joints by means of diffusion welding. Weld Cutting 2004;3:285–90.
[10] Ren JW, Li YJ, Feng T. Microstructure characteristics in the interface zone of Ti/Al diffusion bonding. Mater Lett 2002;56:647–52.
[11] Kimura M, Nakamura S, Kusaka M, Seo K, Fuji A. Mechanical properties of friction welded joint between Ti–6Al–4V alloy and Al–Mg alloy (AA5052). Sci Technol Weld Join 2005;10:666–72.
[12] Katoh K, Tokisue H. Effect of insert metal on mechanical properties of friction welded 5052 aluminum alloy to pure titanium joint. J Jpn Inst Light Met 2004;54:430–5.
[13] Fuji A, Ameyama K, North TH. Influence of silicon in aluminium on the mechanical properties of titanium/aluminium friction joints. J Mater Sci 1995;30:5185–91.
[14] Chen YC, Nakata K. Microstructural characterization and mechanical properties in friction stir welding of aluminum and titanium dissimilar alloys. Mater Des 2009;30:469–74.
[15] Chen Y, Ni Q, Ke L. Interface characteristic of friction stir welding lap joints of Ti/Al dissimilar alloys. Trans Nonferr Met Soc 2012;22:299–304.
[16] Dressler U, Biallas G, Alfaro Mercado U. Friction stir welding of titanium alloy TiAl6V4 to aluminium alloy AA2024-T3. Mater Sci Eng A 2009;526:113–7.
[17] Bang KS, Lee KJ, Bang HS, Bang HS. Interfacial microstructure and mechanical properties of dissimilar friction stir welds between 6061-T6 aluminum and Ti–6%Al–4%V alloys. Mater Trans 2011;52:974–8.
[18] Aonuma M, Nakata K. Dissimilar metal joining of 2024 and 7075 aluminium alloys to titanium alloys by friction stir welding. Mater Trans 2011;52:948–52.
[19] Chen Y, Yu L, Ni Q. Influence of zinc on the microstructure and brittle phases of friction stir welded joint of Al/Ti dissimilar alloys. Adv Mater Res 2012;413:439–43.
[20] Wei Y, Li J, Xiong J, Huang F, Zhang F, Raza SH. Joining aluminum to titanium alloy by friction stir lap welding with cutting pin. Mater Charact 2012;71:1–5.
[21] ISO/TR 16060:2003, Destructive tests on welds in metallic materials–– etchants for macroscopic and microscopic examination. International Organization for Standardization; 2003.
[22] ISO 6892:1998, Metallic materials—tensile testing at ambient temperature. International Organization for Standardization; 1998.
[23] Sauvage X, Dédé A, Muñoz AC, Huneau B. Precipitate stability and recrystallisation in the weld nuggets of friction stir welded Al–Mg–Si and Al–Mg–Sc alloys. Mater Sci Eng A 2008;491:364–71.
[24] Sato Y, Kokawa H, Enomoto M, Jogan S. Microstructural evolution of 6063 aluminum during friction-stir welding. Met Mater Trans A 1999;30:2429–37.
[25] Elangovan K, Balasubramanian V, Valliappan M. Effect of tool pin profile and tool rotational speed on mechanical properties of friction stir welded AA6061 aluminium alloy. Mater Manuf Processes 2008;23:251–60.

[26] Mishra RS, Ma ZY. Friction stir welding and processing. Mater Sci Eng R 2005;50:1–78.
[27] Threadgill PL, Leonard AJ, Shercliff HR, Withers PJ. Friction stir welding of aluminium alloys. Int Mater Rev 2009;54:49–93.
[28] Ren SR, Ma ZY, Chen LQ. Effect of welding parameters on tensile properties and fracture behavior of friction stir welded Al–Mg–Si alloy. Scr Mater 2007;56:69–72.
[29] Liao JS, Yamamoto N, Liu H, Nakata K. Microstructure at friction stir lap joint interface of pure titanium and steel. Mater Lett 2010;64:2317–20.
[30] Liu FC, Ma ZY. Influence of tool dimension and welding parameters on microstructure and mechanical properties of friction-stir-welded 6061-T651 aluminum alloy. Met Mater Trans A 2008;39:2378–88.